Functional connections between optic flow areas and navigationally responsive brain regions during goal-directed navigation

Katherine R. Sherrill [a,b], Elizabeth R. Chrastil [a,b], Robert S. Ross [c], Uğur M. Erdem [a], Michael E. Hasselmo [a], Chantal E. Stern [a,b,*]

[a] Center for Memory and Brain, Department of Psychological and Brain Sciences, Boston University, Boston, MA 02215, USA
[b] Athinoula A. Martinos Center for Biomedical Imaging, Massachusetts General Hospital, Charlestown, MA 02129, USA
[c] Department of Psychology, University of New Hampshire, Durham, NH 03824, USA

ARTICLE INFO

ABSTRACT

Recent computational models suggest that visual input from optic flow provides information about egocentric (navigator-centered) motion and influences firing patterns in spatially tuned cells during navigation. Computationally, self-motion cues can be extracted from optic flow during navigation. Despite the importance of optic flow to navigation, a functional link between brain regions sensitive to optic flow and brain regions important for navigation has not been established in either humans or animals. Here, we used a beta-series correlation methodology coupled with two fMRI tasks to establish this functional link during goal-directed navigation in humans. Functionally defined optic flow sensitive cortical areas V3A, V6, and hMT+ were used as seed regions. fMRI data was collected during a navigation task in which participants updated position and orientation based on self-motion cues to successfully navigate to an encoded goal location. The results demonstrate that goal-directed navigation requiring updating of position and orientation in the first person perspective involves a cooperative interaction between optic flow sensitive regions V3A, V6, and hMT+ and the hippocampus, retrosplenial cortex, posterior parietal cortex, and medial prefrontal cortex. These functional connections suggest a dynamic interaction between these systems to support goal-directed navigation.

© 2015 Elsevier Inc. All rights reserved.

Introduction

Utilization of self-motion cues during first person perspective navigation to track changes in position and orientation relies heavily on the accurate perception of optic flow, the pattern of relative visual motion between the observer and environment. Humans and animals are able to spatially code their movement by monitoring self-motion to track changes in position and orientation, mechanisms that comprise a process known as path integration (McNaughton et al., 2006; Wolbers et al., 2007; Chrastil, 2013; Arnold et al., 2014). It has been proposed that optic flow is important for path integration because it provides information about the navigator's movement through the environment (Kearns et al., 2002; Hasselmo, 2009; Tcheang et al., 2011; Raudies et al., 2012). fMRI and psychophysical experiments have used optic flow localizers to identify human cortical areas selective for processing flow motion, including areas V3A and V6 (Tootell et al., 1997; Seiffert et al., 2003; Cardin and Smith, 2010; Pitzalis et al., 2006, 2010) and the human motion complex (hMT+) (Tootell et al., 1997; Seiffert et al., 2003; Duffy, 2009). Functional connections between brain regions

sensitive to optic flow and navigationally responsive regions may support successful navigation in sparse, landmark-free environments, in which self-motion cues play an important role.

Spatially tuned cells in the rodent represent position and head orientation during navigation. Hippocampal place cells increase their firing rates during movement in specific locations in their environment (O'Keefe and Dostrovsky, 1971), entorhinal grid cells code arrays of locations (Hafting et al., 2005), and head direction cells are tuned to specific heading directions (Taube et al., 1990). Computational models have used external cues from the environment to drive persistent spiking of head direction cells, which update grid cell responses that, in turn, update hippocampal place cell activity (Hasselmo, 2009) (Fig. 1). Alternatively, optic flow can drive border cells that directly drive place cells or place cells could be driven by egocentric (navigator-centered) angle of visual features combined with knowledge of allocentric (environment-centered) head direction. Recent models indicate that visual input from optic flow provides information about egocentric motion and influences firing patterns in spatially tuned cells including border cells during rodent navigation (Raudies et al., 2012; Raudies and Hasselmo, 2012). Head direction cells have been found in the rodent retrosplenial cortex (Chen et al., 1994; Cho and Sharp, 2001), suggesting that this region could support updating head orientation during movement. Since previous rodent research indicates that the hippocampus

* Corresponding author at: Center for Memory and Brain, Boston University, 2 Cummington Mall, Room 109, Boston, MA 02215, USA.
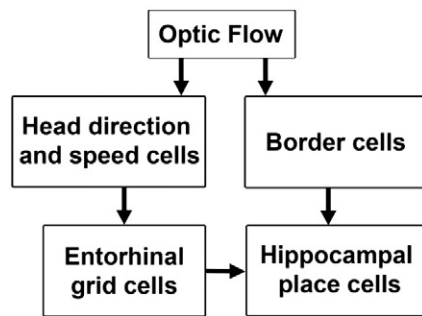E-mail address: Chantal@bu.edu (C.E. Stern).

Fig. 1. Simplified model adapted from Hasselmo (2009) depicting how optic flow input influences spatially tuned cells. Optic flow information drives head direction cells to maintain the direction and speed of a trajectory. Head direction and speed cells drive grid cell responses in the entorhinal cortex that in turn update place cells in the hippocampus. Alternatively, optic flow can also influence border cell activity (Raudies and Hasselmo, 2012), and border cells can directly update place cell responses (Hartley et al., 2000).

and retrosplenial cortex support position and head orientation updating, these areas may be functionally connected with optic flow sensitive regions during navigation relying on self-motion cues. However, a functional link between brain regions sensitive to optic flow and navigationally responsive regions has not yet been established in animals or humans. Based on these animal and computational models, we predicted that regions sensitive to optic flow – areas V3A, V6, and hMT+ – would be functionally connected with navigationally responsive regions, including hippocampus and retrosplenial cortex, during first person navigation in humans.

In the current fMRI study, we localized cortical brain regions responsive to optic flow motion and then determined whether these regions were functionally connected with navigationally responsive brain regions identified during first person perspective (FPP) navigation. The functional connectivity methods we employed (Rissman et al., 2004) rely on the assumption that a correlation of the BOLD signal between regions of interest and other regions of the brain indicates a functional interaction between the regions. A significant functional connection suggests a task-dependent coherence between regions based on trial-by-trial BOLD fluctuations relating to the task. This method does not imply that there is a direct anatomical connection between two brain regions. Since 2004 (Rissman et al., 2004), the beta series correlation method has been used extensively across a variety of different cognitive processes, from interregional interactions during working memory and navigational paradigms (Gazzaley et al., 2007; Brown et al., 2012) to establishing functional connections during resting state that mirror known structural connectivity (Greicius et al., 2009; Scholvinck et al., 2010), to characterizing brain connectivity in clinical populations (Lesh et al., 2011; Fornito et al., 2012).

In our navigation task, participants viewed a map of a landmark-deprived environment indicating the start and goal locations and then utilized these survey-level spatial representations to actively navigate the environment in either FPP or Survey (Bird's eye) perspectives (Sherrill et al., 2013). The goal of this study was to examine functional connections between brain regions sensitive to optic flow (areas V3A, V6, and hMT+) and brain regions that support spatial navigation in humans, including the hippocampus and retrosplenial cortex, thus providing evidence for a link between empirical and computational models of navigation.

Methods and materials

Participants

Twenty-three participants were recruited for this study from the Boston University community. All participants were right-handed and had self-reported experience playing video games. Written informed consent was obtained from each participant prior to enrollment in

accordance with the experimental protocol approved by both the Boston University Charles River Campus Institutional Review Board and the Partners Human Research Committee.

Three participants were eliminated from the final analysis due to excessive motion during functional magnetic resonance imaging (fMRI) scanning while two additional participants were eliminated due to technical issues during the scanning sessions. Each participant completed a navigation task designed to examine goal-directed navigation using path integration mechanisms (Sherrill et al., 2013) and an optic flow paradigm contrasting coherent and egocentric flow field visual motion with non-coherent, random motion processing (Seiffert et al., 2003; Pitzalis et al., 2010; Putcha et al., 2014). Our whole-brain analysis included participants who scored at least 50% correct on all trials in each perspective of the navigation task in order to maintain a minimum number of correct trials for analysis. Four participants were excluded due to poor performance on the navigation task. Fourteen participants were included in the final functional connectivity analysis (mean age 23.214 ± 3.26 (SD); 9 males, 5 females).

Virtual navigation task environment

Detailed information about the navigation paradigm can be found in our earlier fMRI publication (Sherrill et al., 2013). Briefly, participants were shown a survey representation of their start location, heading direction, and a goal location. Following a delay, the participants actively navigated to the encoded goal location using a button box. Panda3D Software (Entertainment Technology Center, Carnegie Mellon University, PA) was used to create a virtual environment consisting of an open field extending in all directions towards the horizon and sky (orthographic lens, 130 × 130 film size) (Fig. 2). There were no distal landmarks or distinguishing proximal landmarks that participants could use to orient themselves within the environment. One virtual unit represented 0.5 m in the virtual environment. Short, circular columns (radius six virtual units, height 0.15 virtual units) were placed upon the floor of the open field to prevent participants from moving directly to the goal location. Thus, navigational routes arced around the columns, encouraging active computation and maintenance of orientation.

Participants navigated through the environment using a button response box. Navigation occurred in one of three visual perspectives: first person perspective (FPP), third person perspective (TPP), or Survey perspective (Fig. 2). For the current study, FPP and Survey perspectives were included in the analysis (see Sherrill et al., 2013 for univariate results for FPP vs. TPP navigation). In both perspectives, movement speed was held constant at 5 virtual units per second. In the FPP, the participant's perspective was set at a height of two virtual units. The field of view during FPP navigation was restricted to the scene in front of the participant, consistent with the definition of first person perspective. Optic flow was representative of what a person walking through the environment would experience. In the Survey perspective, the participant steered a vehicle to the goal location from a fixed, survey-level perspective looking directly down at the 0,0,0 coordinate (Fig. 2). Thus, there was no optic flow representative of self-motion during Survey perspective navigation.

Training procedures

One day prior to scanning, participants were trained on the navigation task. In the task, they encoded start and goal locations from a survey-level map perspective and then translated this spatial representation into accurate, goal-directed navigation from a FPP, TPP, or Survey perspective (Sherrill et al., 2013). Participants were informed that following the navigation task they would complete an optic flow paradigm, but no pre-training on the optic flow paradigm was necessary. Participants were given a practice run to refamiliarize themselves with the navigation task and keyboard controls prior to being placed in the scanner.
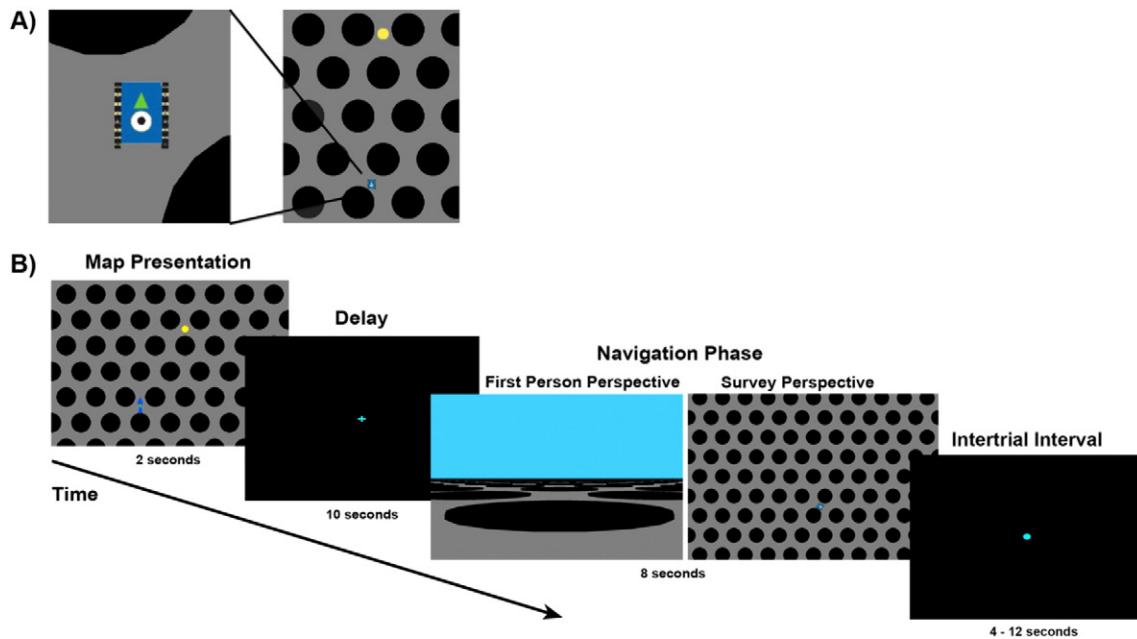
Fig. 2. Navigation task paradigm. A) Survey perspective of the vehicle (blue) that was guided by participants to the goal location (yellow dot). Expanded view displays the vehicle as depicted in the navigation phase with green arrow showing orientation in the environment. B) During the two-second map presentation, participants were shown a survey-level representation of the environment with their start location, heading direction (blue arrow overlaid on vehicle), and goal location clearly marked. Map presentation was followed by a delay, during which participants made no response. Following the delay was an eight second navigation phase requiring active navigation to the goal location in which movement occurred either in the first person perspective (FPP) or a Survey perspective.

Experimental tasks

Navigation task

Each trial consisted of map presentation, delay, and navigation phases, followed by an inter-trial interval (ITI). Trials of the FPP, TPP, and Survey perspective conditions were presented in an interleaved, randomized order. During the two-second map presentation, participants were shown a survey representation of the environment with their start location, heading direction, and goal location clearly marked. The map presentation phase was followed by a ten second delay, during which participants made no response. Following the delay was an eight second navigation phase requiring active navigation to the encoded goal location. Participants were instructed to recall the goal location and navigate to its precise location. The goal location was not visible during the navigation phase, and no feedback was given as to whether the participant successfully reached the goal location. A trial was considered correct if participants' trajectories during the navigation phase came within a radius of three virtual units from the goal location. The distance between the start location and goal location was on average 25.78 ± 1.61 (SD) virtual units across all trials. Therefore, three virtual units correspond to 11.6% of the average distance between the start and goal location. Each navigation phase was followed by an ITI (four to twelve second duration, averaging 8 s) in which participants viewed a fixation point in the center of a black screen. Collinearity between the navigation phase and ITI was reduced by varying the length of the ITI (<0.1), ensuring a high degree of discriminability between phases. Critically, no distinguishing landmarks, distal cues, or goal location markers were present in the environment. This required participants to rely on stimuli such as self-motion cues from optic flow in order to execute their planned route during ground-level navigation. Participants did not know the trial type (FPP, TPP, or Survey perspective navigation) until the start of the navigation phase. During scanning, participants performed ten runs of the navigation task composed of twelve trials per run. The order of the trials was counterbalanced across runs (run duration: 5 min and 52 s; TR = 2 s), and the order of runs was randomized across participants. There were forty trials per trial type.

Optic flow localizer

Following the navigation task, each scanning session included six runs of the functional optic flow localizer. Each functional run (run duration: 4 min and 24 s; TR = 2 s) consisted of 8 cycles of 16-second alternating blocks of flow motion (termed "Flow") and random motion (termed "Random") conditions. The order of the first presentation condition (Flow or Random) alternated across participants. Flow and random motion were created using two thousand moving white dots (each 2 arc-min × 2 arc-min; dot duration = 500 ms) presented within a circular aperture of 10.5° by 16.7° (height × width). Dot density was 4.14 dots per cm². Dot speed was scaled with the radial distance from the focus of expansion/contraction. In the flow condition, all dots moved with a coherent expansion/contraction direction and/or consistent rotation direction about the central fixation cross. The expansion and contraction of optic flow changed several times per block of the Flow condition. Eight mini-blocks were included for each flow condition block, alternating between clockwise and counterclockwise flow during inward and outward contraction/expansion movement of dots (Fig. 3A). In the random condition, the dot speed was equivalent to the flow condition, yet the direction of dot movement was random, without a coherent direction or center of expansion/contraction (Fig. 3B). Participants were instructed for all conditions to maintain fixation on a small crosshair in the center of the screen. The optic flow task used here was based on the task developed by and described in Pitzalis et al. (2010). Visual stimuli were presented with VisionEgg (Straw, 2008) and were projected onto a rear-projection screen.

Image acquisition

Images were acquired at the Athinoula A. Martinos Center for Biomedical Imaging, Massachusetts General Hospital in Charlestown, MA using a 3 T Siemens MAGNETOM TrioTim scanner with a 32-channel Tim Matrix head coil. A high-resolution T1-weighted multi-planar rapidly acquired gradient echo (MP-RAGE) structural scan was acquired using Generalized Autocalibrating Partially Parallel Acquisitions
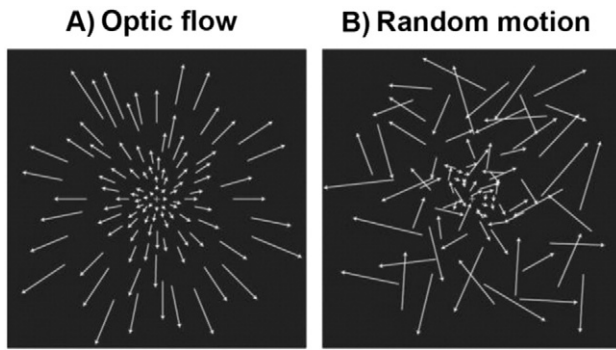
A) Optic flow   B) Random motion

Fig. 3. Optic flow stimuli depiction. The length of the arrows corresponds with dot speed; dot speed increases with greater distance from the center focus. A) Illustration of optic flow motion (Flow) stimuli that simulated coherent motion using dot fields. This example motion field depicts expansion optic flow motion simulating forward self-motion. Motion fields could also show contraction optic flow motion simulating backward motion, clockwise radial flow induced by counterclockwise rotation about a center focus, or counterclockwise rotation induced by clockwise rotation about a center focus. B) Illustration of non-coherent motion (Random) stimuli using dots moving at the same speeds as the Flow condition, but the direction of movement is random.

(GRAPPA) (TR = 2530 ms; TE = 3.31 ms; flip angle = 7°; slices = 176; resolution = 1 mm isotropic).

Images for the Navigation task were acquired first. T2*-weighted BOLD images were acquired using an Echo Planar Imaging (EPI) sequence (TR = 2000 ms; TE = 30 ms; flip angle = 85°; slices = 33, resolution = 3.4 × 3.4 × 3.4 mm, interslice gap of 0.5 mm). Functional image slices were aligned parallel to the long axis of the hippocampus.

Images for the optic flow paradigm were acquired immediately following the navigation task; participants were not taken out of the scanner between scans. T2*-weighted BOLD fMRI data was acquired during visual stimuli presentation (TR = 2000 ms; TE = 30 ms; FA = 90°; slices = 32; resolution = 4 × 4 × 4 mm). Functional image slices were aligned parallel to the anterior–posterior commissural line.

fMRI pre-processing

Functional imaging data were preprocessed and statically analyzed using the SPM8 software package (Statistical Parametric Mapping, Wellcome Department of Cognitive Neurology, London, UK). All BOLD images were first reoriented so the origin (i.e. coordinate xyz = [0, 0, 0]) was at the anterior commissure. The images were then corrected for differences in slice timing and were realigned to the first image collected within a series. Motion correction was conducted next and included realigning and unwarping the BOLD images to the first image in the series in order to correct for image distortions caused by susceptibility-by-movement interactions (Andersson et al., 2001). Realignment was estimated using 7th degree B-spline interpolation with no wrapping while unwarp reslicing was done using 7th degree B-spline interpolation with no wrapping. The high-resolution structural image was then coregistered to the mean BOLD image created during motion correction and segmented into white and gray matter images. The bias-corrected structural image and coregistered BOLD images were spatially normalized into standard Montreal Neurological Institute (MNI) space using the Diffeomorphic Anatomical Registration using Exponentiated Lie algebra (DARTEL) algorithm (Ashburner, 2007) for improved inter-subject registration. BOLD images were resampled during normalization to 2 mm³ isotropic voxels and smoothed using a 6 mm full-width at half-maximum Gaussian kernel. The normalized structural images of all fourteen participants were averaged after normalization for displaying overlays of functional data.

Data analysis

Behavioral data analysis

To compare overall performance between the FPP and Survey perspective experimental conditions, a paired-samples t-test was run comparing accuracy in the two conditions. Behavioral analyses were completed using PASW Statistics 18 (SPSS, Inc., Chicago, IL). Only successful navigation trials were included in the subsequent analyses exploring functional connectivity between optic flow sensitive and navigationally-responsive brain regions.

fMRI analysis

For the optic flow paradigm, trials were analyzed in a block design format. Conditions were classified as either "flow" or "random". Blocks for each condition were constructed as a series of square waves, termed "boxcars". Each block was modeled as a 16-second boxcar defined by the onset of the condition. Analysis was based on a mixed-effects general linear model in SPM8. To capture activation response to coherent flow motion that was not responsive to random motion, contrast images were created contrasting the Flow compared to Random conditions (Flow > Random) within each participant. Group-averaged statistical parametric maps (SPMs) were created by entering the Flow against Random conditions (Flow > Random) contrast images from each participant into a one-sample t-test using participant as a random factor.

For each analysis, a voxel-wise statistical threshold of $p < 0.01$ was applied to the whole brain contrast maps. To correct for multiple comparisons, we applied a cluster-extent threshold technique. The AlphaSim program in the AFNI software package (http://afni.nimh.nih.gov/afni/) was used to conduct a 10,000 iteration, 6 mm autocorrelation Monte Carlo simulation analysis on voxels within the group functional brain space using the ResMS header file (172,761 voxels). From this analysis, a minimum voxel extent of 145 was determined to maintain a family-wise error rate of $p < 0.01$.

fMRI functional connectivity analysis

Region of interest ("seed" region) selection

A group-averaged statistical parametric map of brain regions sensitive to optic flow was generated from the optic flow paradigm contrasting Flow and Random motion (see above). We used this optic flow activation map to localize seed regions for the functional connectivity analysis. Prior neuroimaging studies have identified human cortical areas that are responsive to optic flow motion, specifically visual cortical areas V3A and V6 and hMT+. Area V3A, located inferior to the parieto-occipital sulcus, is highly selective for processing visual motion (Tootell et al., 1997; Seiffert et al., 2003; Pitzalis et al., 2010). Human area V6, like macaque area V6, is located in the dorsal parieto-occipital sulcus (Pitzalis et al., 2006). Area V6 in humans has been described as selectively responding to expanding egocentric flow field visual motion information in humans, which simulates forward motion (Pitzalis et al., 2006, 2010; Cardin and Smith, 2010). Macaque studies have established that the medial superior temporal (MST) area accounts for heading information derived from optic flow, suggesting a role in self-motion processing based on visual cues (Logan and Duffy, 2006; Bremmer et al., 2010). The human motion complex (hMT+), a homolog of macaque area MST (Dukelow et al., 2001; Huk et al., 2002), is located in the posterior region of the middle temporal gyrus and is activated by subjects making estimates of heading direction (Peuskens et al., 2001) and has been characterized as extracting coherent motion cues selective for self-motion (Rust et al., 2006; Cardin and Smith, 2010, 2011; Pitzalis et al., 2010).

Seed regions were drawn as 5 mm spherical ROIs centered on a peak activated voxel in the flow motion SPM (Flow > Random). The V3A seed region was centered on peak coordinates (Left: −16,−84,24; Right: 22,−84,20), and the V6 seed region was centered on peak coordinates (Left: −12,−80,32; Right: 22,−84,32), as shown in Fig. 4. The hMT+
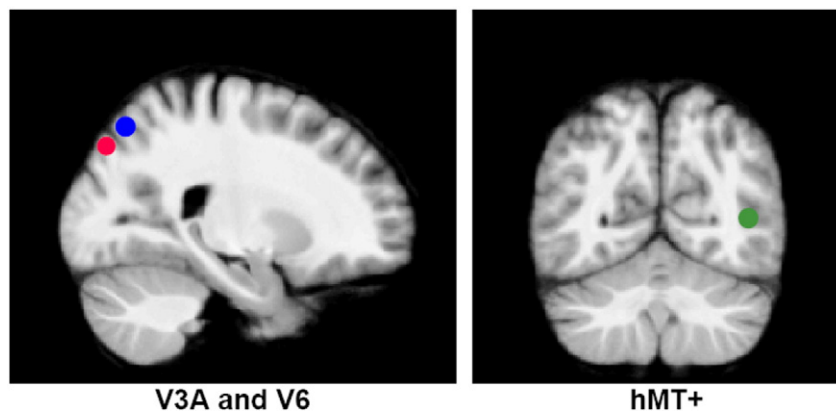
Fig. 4. Functional connectivity seed regions. Seed region locations based on brain areas activated during the optic flow paradigm contrasting Flow and Random motion (Flow > Random). Red and blue circles indicate bilateral visual cortical areas V3A and V6 seed regions, respectively. The seed region in the right human motion complex (hMT+) is shown in green.

seed region was centered on peak coordinates $(44, -62, 2)$ from our whole brain activation map for flow motion (Flow > Random) (Fig. 4). Our hMT+ seed region has similar coordinates to a human fMRI study in which hMT+ was activated during a triangle completion path integration task (Wolbers et al., 2007). Although our optic flow task significantly activated bilateral hMT+ regions at a lower statistical threshold ($p < 0.05$), only the right hMT+ region survived our strict cluster correction of the Flow motion SPM (Flow > Random) ($p < 0.01$ voxel extent with $p < 0.01$ cluster significance); therefore, a right hemisphere seed region was specified in our analysis. Our seed regions were consistent in anatomical location with boundaries described in previous neuroimaging studies (Tootell et al., 1997; Swisher et al., 2007; Wandell et al., 2007; Wolbers et al., 2007; Pitzalis et al., 2010; Putcha et al., 2014).

Beta series correlation analysis

Functional connectivity analyses were conducted using the beta series correlation analysis method (Rissman et al., 2004), which our lab has used previously in memory and navigation studies (Ross et al., 2009; Brown et al., 2012). The beta series correlation method utilizes the univariate fMRI data analysis so that parameter estimates, or beta weights, reflecting the magnitude of the task-related blood oxygen level dependent (BOLD) responses are estimated for each trial. Therefore, the beta series correlation analysis requires that the individual trials of events examined in the functional connectivity analysis be modeled separately. The beta series correlation functional connectivity analysis method relies on the assumption that the degree of similarity (correlation strength) between the fluctuations of parameter estimates across trials extracted from regions of interest serves as a metric of the functional interaction between the regions (Rissman et al., 2004). Two brain regions (for example, an optic flow responsive region and a navigationally responsive region) may both significantly increase their activation, on average, across trials for a particular experimental manipulation, but still lack any coherence between their trial-by-trial responses to the task. Conversely, it is possible for a brain region to have significant task-dependent coherence across trials with another region, without necessarily increasing its average activity level. Using the beta series correlation functional connectivity analysis method, we determined correlations of our respective seed regions' beta series with the beta series of all other voxels in the brain for the navigation phase and intertrial interval (ITI). The beta series correlation analysis generates raw correlation (r) maps, which are transformed into z-maps. For more details and validation of the beta-series correlation method, see Rissman et al. (2004).

Our functional connectivity analysis was restricted to two phases of the task, the navigation phase and the intertrial interval (ITI). Our interest was in analyzing successful navigation, so only trials in which the participant successfully reached the goal location were included. The individual trials for the navigation phase and ITI for successful trials in each condition (FPP or Survey perspective) were modeled separately with their own regressor for inclusion in the functional connectivity analysis. The number of regressors in each participant's model varied based on the number of successful trials in each condition, but there were the same number of regressors for the navigation phase and ITI for a given condition. Because there were 40 trials per condition (FPP or Survey perspective navigation), a participant with 100% performance on the task would have 40 successful FPP navigation phase regressors, 40 ITI regressors from successful FPP navigation trials, 40 successful Survey navigation phase regressors, and 40 ITI regressors from successful Survey navigation trials.

To accurately capture variance within the task, all other covariates of non-interest were collapsed into regressors based on condition, task phase, and trial success, similar to modeling for a traditional univariate fMRI analysis. Trials in which the participant was unsuccessful in navigating to the goal location were modeled into 4 regressors to represent unsuccessful trials during the navigation phase and ITI for the FPP and Survey conditions. Two additional time periods of the task were modeled: the map presentation and the delay period. These two factors were each separately modeled with four regressors: successful trials in the FPP condition, unsuccessful trials in the FPP condition, successful trials in the Survey condition, and unsuccessful trials in the Survey condition. Data was also collected for trials in which navigation occurred from a third person perspective (TPP) (Sherrill et al., 2013), but for the current study, only FPP and Survey perspective trials were used. To accurately capture any variance due to the presence of TPP trials, 8 regressors were included for the successful and unsuccessful trials phases (Map Presentation, Delay, Navigation Phase, and ITI) for the TPP condition. Finally, the six motion parameters calculated during motion correction were added to the model as additional covariates of no interest. In total, a participant with 100% successful trials would have a design matrix containing 182 regressors (160 for the beta series correlation analysis of the navigation phase and ITI of FPP and Survey conditions, and 22 regressors for remaining task components and noise sources). Regressors from the task were modeled as square waves, or "boxcars". Boxcar onsets were defined by the onset of each event and extended for the duration of the event (eight seconds for the Navigation Phase and a four to twelve second variable duration for the ITI). These parameters were convolved with the canonical hemodynamic response function in SPM8.

Participant-specific parameter estimates were calculated for each regressor using the least squares solution of the general linear model (GLM) approach in SPM8. An SPM8 default 0.008 Hz high-pass filter was used during first level model specification to remove very slow drifts in signal over time. The parameter estimates for trials within each condition of interest were concatenated to form a "beta series". The beta series functional connectivity method assumes that the degree of similarity (correlation strength) between the fluctuations of

parameter estimates across trials between two voxels serves as a metric for the functional interaction between the voxels. Using a custom MATLAB (MathWorks, Natick, MA) script (Rissman et al., 2004), we determined correlations between the respective beta series for our seed regions of visual regions V3A and V6 and hMT+ and all other voxels in the brain during the navigation phase and ITI for the FPP and Survey conditions. Condition-specific whole brain correlation maps were obtained by calculating the correlation of the seed region's beta series with that of all other voxels in the brain. The beta series correlation analysis generates raw correlation (r) maps, which are then transformed into z maps using an arc-hyperbolic tangent transform to allow statistical comparisons between correlation magnitudes.

Functional connectivity specifically related to successful navigation in either the FPP and Survey perspective was assessed by comparing the navigation phase z-transformed correlation maps to the ITI z-transformed correlation maps for each individual participant using paired t-tests in SPM8 (i.e. FPP navigation phase > FPP ITI). For each analysis, a voxel-wise statistical threshold of $p < 0.01$ was applied to the whole brain contrast maps. To correct for multiple comparisons, we applied a cluster-extent threshold technique. The AlphaSim program in the AFNI software package (http://afni.nimh.nih.gov/afni/) was used to conduct a 10,000 iteration, 6 mm autocorrelation Monte Carlo simulation analysis on voxels within the group functional brain space using the ResMS header file (176,189 voxels). From this analysis, a minimum voxel extent of 145 was determined to maintain a family-wise error rate of $p < 0.01$.

Results

Behavioral data

We examined navigation performance and accuracy when navigating in both the first person perspective (FPP) and Survey perspectives.

Participants reached within 3 virtual units of the goal in the FPP in 71.61% of the trials (SEM 3.81) and the Survey perspective in 79.29% of the trials (SEM 3.24). A paired-samples t-test revealed a significant difference in accuracy between the FPP and Survey perspectives ($t_{(13)} = 2.895$, $p < 0.05$). Participants navigated to the goal location in 6.32 ± 0.06 (SD) seconds on average across all trials.

fMRI connectivity data

To examine functional connections during successful navigation, all results discussed are comparisons of the navigation phase against the intertrial interval (ITI) for successful trials. Complete listings of significant functional connectivity differences during successful navigation from either the FPP or Survey perspective by seed region are shown in Tables 1, 2, and 3.

Functional connections with optic flow sensitive regions during first person perspective navigation

In the virtual environment, participants had to integrate optic flow motion cues to accurately monitor the spatial relationship of their current position and the goal location during navigation. During FPP navigation compared with the ITI, increased functional connectivity was observed between regions of the brain that are sensitive to optic flow motion and the retrosplenial cortex, posterior parietal cortex, hippocampus, and medial prefrontal cortex, which are brain regions previously noted in human navigational studies (Wolbers et al., 2007; Spiers and Maguire, 2007; Brown et al., 2010; Baumann and Mattingley, 2010; Doeller et al., 2010; Brown and Stern, 2014; Sherrill et al., 2013). For a summary of all brain regions showing significant functional connectivity with V3A, V6, and hMT+ seed regions at the whole-brain level for FPP navigation, see Tables 1, 2, and 3, respectively.

Table 1
Brain regions functionally connected with left and right V3A seed regions during navigation from the first person perspective (FPP) and Survey perspective compared with ITI. MNI coordinates reflect cluster-center voxels. T-values reflect a statistical threshold of $p < 0.01$. Activation clusters survived cluster-threshold correction for multiple comparisons to $p < 0.01$ with a minimum cluster size of 145 voxels.

Contrast	Seed region	Area	Left		Right	
			T	MNI x,y,z (mm)	T	MNI x,y,z (mm)
FPP navigation Phase > ITI	Left V3A	Hippocampus (head)	4.05	−28,−12,−20	2.81	24,−8,−24
		Hippocampus (body)	2.69	−28,−24,−14	3.92	32,−18,−16
		Retrosplenial cortex	5.80	−2,−52,18	2.81	4,−50,14
		Posterior parietal cortex	2.88	−2,−56,30	4.87	4,−54,30
		Precuneus	5.49	−6,−46,34	3.14	10,−50,34
		Superior parietal lobule	4.83	−36,−74,50		
		Angular gyrus	5.85	−54,−68,26	5.15	50,−48,28
		Medial prefrontal cortex	4.08	−2,54,−4	4.45	4,58,6
		Orbitofrontal gyrus	4.61	−26,36,−12	6.72	30,36,−12
		Superior frontal gyrus (BA 9)	10.66	−10,64,26	6.38	14,56,34
		Superior frontal gyrus (BA 6)	7.09	−10,30,52	6.28	24,40,50
		Inferior frontal gyrus (BA 44/45)	6.63	−52,20,−4		
		Insula	4.44	−34,6,−8	5.47	32,8,−10
		Amygdala	4.43	−16,−10,−18	3.98	24,−2,−18
		Middle temporal gyrus/temporal pole	5.43	−44,14,−40	4.76	52,8,−34
	Right V3A	Retrosplenial cortex	4.00	−4,−50,10	5.23	2,−52,16
		Precuneus	5.16	−2,−52,34	3.70	4,−56,38
		Superior parietal lobule	3.82	−34,−74,48		
		Angular gyrus	6.74	−54,−66,24	4.43	48,−50,24
		Medial prefrontal cortex	4.44	−4,52,−6	5.42	2,54,−12
		Superior frontal gyrus (BA 9)	6.29	−6,58,22	5.92	8,56,34
		Middle temporal gyrus/temporal pole	6.52	−46,14,−32	8.82	52,8,−36
Survey navigation Phase > ITI	Left V3A	Primary motor cortex/precentral gyrus			6.33	30,−16,70
		Insula			5.25	52,2,6
		Inferior frontal gyrus			4.68	64,−6,14
	Right V3A	Primary motor cortex/precentral gyrus	3.76	−12,−32,64	4.28	22,−28,72
		Hippocampus (body)			6.14	22,−20,−16
		Medial prefrontal cortex			3.20	4,52,−6
		Paracentral gyrus	4.33	−4,−28,58	3.51	6,−26,60

Table 2
Brain regions functionally connected with left and right V6 seed regions during navigation from the first person perspective (FPP) and Survey perspective compared with ITI. MNI coordinates reflect cluster-center voxels. T-values reflect a statistical threshold of $p < 0.01$. Activation clusters survived cluster-threshold correction for multiple comparisons to $p < 0.01$ with a minimum cluster size of 145 voxels.

Contrast	Seed region	Area	Left		Right	
			T	MNI x,y,z (mm)	T	MNI x,y,z (mm)
FPP navigation Phase > ITI	Left V6	Hippocampus (head)			3.15	24,−16,−18
		Hippocampus (body)			3.25	24,−26,−12
		Retrosplenial cortex	4.45	−6,−52,16	2.69	6,−50,14
		Posterior parietal cortex	4.01	−2,−64,28	4.34	6,−54,26
		Precuneus	3.35	−4,−52,34	4.05	4,−50,32
		Angular gyrus	6.18	−54,−66,24	5.12	52,−48,26
		Medial prefrontal cortex	4.03	−4,56,−6	3.22	2,50,0
		Insula			3.87	46,−10,16
		Superior frontal gyrus (BA 9)	4.69	−12,62,24	3.98	8,56,34
		Amygdala			3.18	18,−6,−16
		Middle temporal gyrus/temporal pole			5.13	52,6,−34
		Superior temporal gyrus			4.10	56,6,−12
		Lateral occipital gyrus	3.25	−58,−64,12	8.39	58,−62,12
	Right V6	Hippocampus (head)			3.15	24,−10,−22
		Hippocampus (body)			2.76	30,−20,−18
		Retrosplenial cortex	3.46	−2,−50,16	3.58	2,−52,18
		Precuneus	3.23	−6,−48,34	3.14	−6,−46,34
		Angular gyrus	5.85	−56,−64,24	5.98	52,−66,38
		Medial prefrontal cortex	5.27	−6,62,−4	4.79	8,56,−12
		Orbitofrontal cortex	3.77	−26,36,−12		
		Superior frontal gyrus (BA 9)	6.41	−4,54,36	4.44	8,58,32
		Inferior frontal gyrus	5.56	−48,30,−4		
		Middle temporal gyrus/temporal pole	5.78	−58,0,−22	6.57	56,12,−32
Survey navigation Phase > ITI	Left V6	Primary motor cortex/precentral gyrus	5.82	−12,−30,66	5.67	14,−26,64
		Paracentral gyrus	3.84	−6,−26,66	4.35	6,−28,62
		Insula	3.72	−38,−22,18	5.25	36,−2,18
		Middle temporal gyrus			3.33	62,4,−20
		Superior temporal gyrus			4.21	60,−6,−4
	Right V6	Primary motor cortex/precentral gyrus			6.88	12,−24,70
		Insula			5.81	36,−20,14
		Precentral gyrus			7.24	16,−26,72
		Paracentral gyrus	4.92	−6,−26,66	4.37	6,−26,62

V3A connectivity. We observed significant functional connectivity between our V3A seed regions and brain regions recruited during FPP navigation. Left V3A was significantly connected with the head and body of the left and right hippocampus and the bilateral posterior parietal cortex during FPP navigation compared to the ITI (Fig. 5A). Left and right V3A seed regions were both functionally connected with bilateral retrosplenial cortex and bilateral medial prefrontal cortex during FPP navigation (Fig. 5A). The results suggest visual motion processing region V3A is functionally connected with the hippocampus, retrosplenial cortex, posterior parietal cortex, and medial prefrontal cortex during FPP navigation.

V6 connectivity. Our results demonstrate that the V6 seed regions are functionally connected with brain regions recruited during successful goal-directed navigation. Left and Right V6 seed regions were both significantly connected with the head and body of the right hippocampus during FPP navigation compared to the ITI (Fig. 5B). Additionally, left and right V6 seed regions were functionally connected with bilateral

Table 3
Brain regions functionally connected with right human motion complex seed region during navigation from the first person perspective (FPP) and Survey perspective compared with ITI. MNI coordinates reflect cluster-center voxels. T-values reflect a statistical threshold of $p < 0.01$. Activation clusters survived cluster-threshold correction for multiple comparisons to $p < 0.01$ with a minimum cluster size of 145 voxels.

| Contrast	Seed region	Area	Left		Right	
			T	MNI x,y,z (mm)	T	MNI x,y,z (mm)
FPP navigation Phase > ITI	Right hMT+	Hippocampus (head)			4.66	28,−6,−24
		Hippocampus (body)			3.48	28,−24,−16
		Retrosplenial cortex	3.03	−2,−54,12	5.23	4,−50,18
		Posterior parietal cortex	4.61	−2,−64,26	3.78	4,−58,34
		Precuneus	3.36	−4,−54,34	4.35	4,−50,36
		Superior parietal lobule			4.48	40,−26,58
		Angular gyrus	6.85	−46,−72,38	5.67	56,−60,30
		Posterior cingulate gyrus	4.68	−4,−34,36	3.60	6,−30,34
		Medial prefrontal cortex	6.50	−2,46,−4	6.16	2,48,−6
		Orbitofrontal cortex	5.08	−34,38,−14		
		Superior frontal gyrus (BA 9)	4.40	−10,54,34	7.35	10,54,36
		Insula			5.02	40,−10,10
		Middle temporal gyrus/temporal pole	6.42	−46,14,−34	10.52	54,6,−36
Survey navigation Phase > ITI	Right hMT+	Primary motor cortex/precentral gyrus			4.05	36,−16,64
		Superior parietal lobule			4.42	38,−22,48
		Paracentral gyrus	5.27	−6,−24,64	6.05	8,−26,66
		Middle temporal gyrus/temporal pole			3.63	60,4,−20
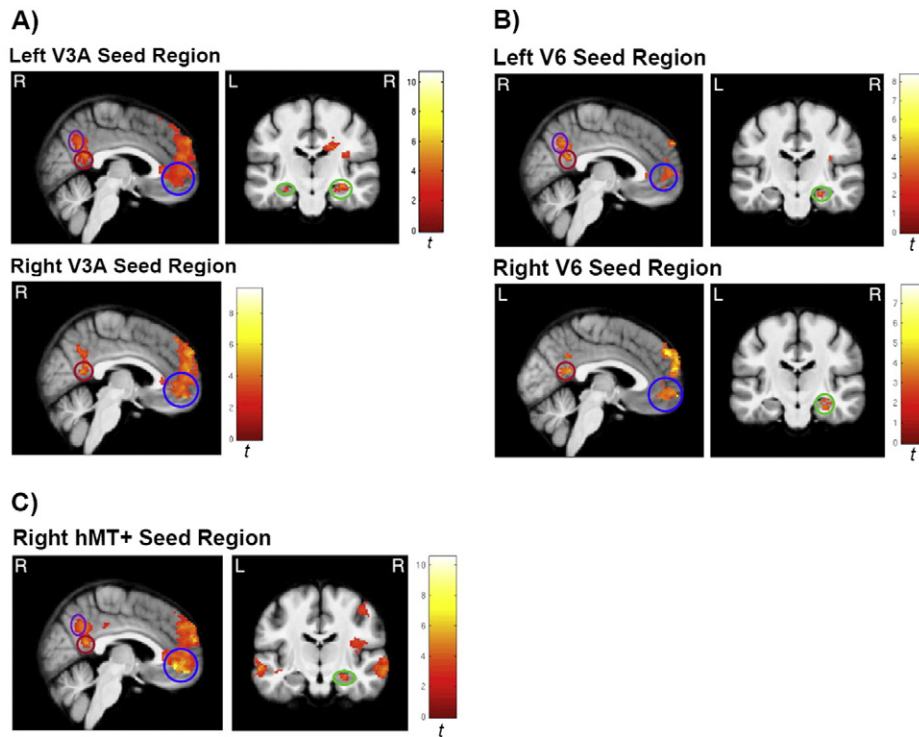
Fig. 5. Optic flow sensitive regions are functionally connected with brain regions supporting first person perspective (FPP) navigation. Sagittal and coronal images of regions functionally connected with A) The left and right V3A seed regions during FPP navigation. B) The left and right V6 seed regions during FPP navigation. C) The right hMT + seed region during FPP navigation. Green circles indicate hippocampal activations. Red circles indicate retrosplenial cortex (RSC) activations. Purple circles indicate posterior parietal cortex (PPC) activations. Blue circles indicate medial prefrontal cortex (mPFC) activations. Functional connectivity analysis images have a statistical threshold of $p < 0.01$ corrected for multiple comparisons with a cluster extent of 145 voxels.

retrosplenial cortex and bilateral medial prefrontal cortex during successful FPP navigation (Fig. 5B). Finally, the left V6 seed region was functionally connected with the bilateral posterior parietal region. These findings further support the functional interaction between optic flow sensitive regions, including cortical area V6, and navigationally responsive regions including the hippocampus, retrosplenial cortex, and medial prefrontal cortex.

hMT+ connectivity. During FPP navigation requiring self-motion cues from optic flow to update position in the environment, functional connections were found between the human motion complex (hMT+) and brain regions recruited for successful goal-directed navigation. Increased functional connectivity was found between the right hMT+ seed and the right head and body of the hippocampus during successful FPP navigation in which the participant successfully reached the goal location compared to the ITI (Fig. 5C). Bilateral retrosplenial cortex, posterior parietal cortex, and medial prefrontal cortex were also functionally connected with the right hMT+ seed region. These results suggest optic flow sensitive region hMT+ is functionally connected with the hippocampus, retrosplenial cortex, and posterior parietal cortex during FPP navigation.

Functional connections with optic flow sensitive regions during Survey perspective navigation

During the Survey perspective navigation phase, visual flow was minimal as the vehicle driven by our participants was the only movement simulated on the screen. From the Survey perspective, the participant was able to see a large portion of the environment and the vehicle they were controlling from a high vantage point. Tracking position in the environment via self-motion cues was not required in the Survey perspective in contrast to its use in FPP navigation. Instead, simply processing the visual scene and making motor responses was all that was required for participants to successfully navigate to an encoded goal location. Our results demonstrate increased functional connectivity between visual cortical areas V3A, V6, and hMT+ and primary and supplementary motor cortices during Survey perspective navigation compared to the ITI (Fig. 6). This finding was not unexpected since we contrasted the navigation phase, which required button responses to navigate, with an intertrial interval in which button responses were not performed. The results also demonstrate that the right V3A seed region was significantly connected with the body of the right hippocampus and the medial prefrontal cortex during Survey perspective navigation compared to the ITI (Fig. 6A). A summary of brain regions functionally connected with V3A, V6, and hMT+ seed regions at the whole-brain level for successful navigation from the Survey perspective are shown in Tables 1, 2, and 3, respectively.

Discussion

We examined functional connections between optic flow regions V3A, V6, and the human motion complex (hMT+) and navigationally responsive brain regions during first person perspective (FPP) navigation. Perception of egocentric flow motion is a critical aspect of visuospatial cognition, as humans rely on processing of visual input continuously as they navigate through their environment. Computational models indicate that optic flow provides information about egocentric (navigator-centered) motion which influences firing patterns in spatially-tuned cells during rodent navigation (Fig. 1; Raudies et al., 2012; Raudies and Hasselmo, 2012). Here, we demonstrate a functional link between optic flow regions and navigation regions in humans. Specifically, our results demonstrate a significant functional relationship between optic flow sensitive regions V6, V3A, and the human motion complex (hMT+) and areas important for FPP navigation, including the hippocampus, retrosplenial cortex, posterior parietal cortex, and medial prefrontal cortex.
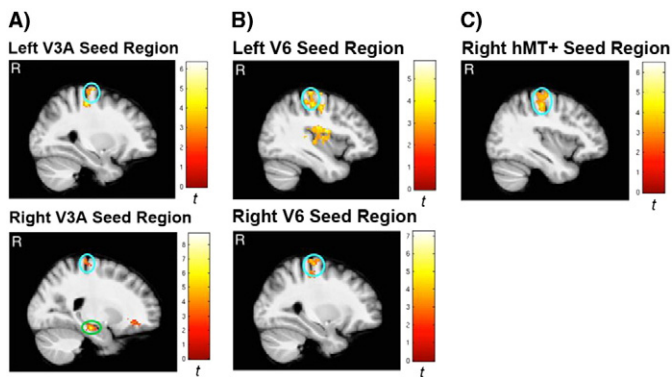
Fig. 6. Optic flow sensitive regions are functionally connected with the primary motor cortices during Survey navigation. Sagittal images of regions functionally connected with A) The left and right V3A seed regions during Survey perspective navigation. B) The left and right V6 seed regions during Survey perspective navigation. C) The right hMT+ seed region during Survey perspective navigation. Light blue circles indicate primary motor cortex activations. Green circles indicate hippocampal activations. Functional connectivity analysis images have a statistical threshold of $p < 0.01$ corrected for multiple comparisons with a cluster extent of 145 voxels.

The role of optic flow responsive areas in processing egocentric movement

Visual information about one's movement in relation to the environment, known as egocentric motion, is essential to track adjustments in position and orientation during navigation. Although other cues for self-motion, such as vestibular input, proprioception, and efferent copies of motor commands, are present during everyday movement, the primary cue for self-motion in virtual environments is optic flow. Previous retinotopic mapping and fMRI studies in humans have established a continuum of several motion-selective regions, including cortical areas V3A, V6, and hMT+ (Tootell et al., 1997; Seiffert et al., 2003; Pitzalis et al., 2006, 2010; Duffy, 2009; Cardin and Smith, 2010). Our optic flow paradigm demonstrated activity within areas V3A, V6, and hMT+, consistent with these earlier studies. These brain regions process coherent flow motion similar to visual input from self-motion cues during first person spatial navigation. Cortical region V3A is highly responsive to processing objective visual motion and discarding self-induced planar retinal motion (Fischer et al., 2012). Cortical region V6 has been characterized as highly selective for coherent motion cues indicative of self-motion (Pitzalis et al., 2010) and is more responsive to egocentric motion than other types of coherent motion (Cardin and Smith, 2010). hMT+ extracts coherent motion cues selective for self-motion and has been implicated in perceiving heading direction (Peuskens et al., 2001). Thus, we predicted a functional link between these optic flow sensitive regions and brain regions recruited for FPP navigation, which depend on self-motion cues to update position and orientation.

Optic flow sensitive regions are functionally connected with brain regions supporting first person perspective navigation

Path integration, the ability to integrate perceived self-motion to update knowledge of current position and orientation, is a fundamental mechanism of spatial navigation. Path integration tracks changes in position and orientation (Wolbers et al., 2007), provides vector knowledge of motion relative to a location (Weiner et al., 2011), and can be used to navigate in an environment towards an intended goal or remembered location (Sherrill et al., 2013; Kalia et al., 2013). Although everyday navigation often relies on landmarks, path integration is an underlying process that updates representations of position and orientation based on self-motion perceptual signals when landmarks may not be present or reliable (May and Klatzky, 2000; Foo et al., 2005). While not necessarily requiring path integration, per se, successful

navigation in the present task relied on similar components, including updating position and orientation to a goal location based on self-motion cues in a landmark-free environment. Our results indicate that optic flow sensitive regions were functionally connected with brain regions recruited during navigation using path integration mechanisms. These results demonstrate significant functional connections between the retrosplenial cortex (RSC) and left and right V3A and V6 and right hMT+ seed regions during FPP navigation. Rodents with RSC lesions exhibit a deficit in path integration when visual cues are not provided, suggesting that the RSC is important for path integration when incorporating visuospatial information with positioning updates (Cooper et al., 2001; Cooper and Mizumori, 2001; Pothuizen et al., 2008; Elduayen and Save, 2014). Head direction cells have also been observed in the rodent RSC (Chen et al., 1994; Cho and Sharp, 2001), suggesting that this region could support tracking head orientation. Recent human neuroimaging studies have indicated the RSC integrates self-motion cues during navigation with route-based spatial information (Wolbers and Buchel, 2005), directs movement towards a goal location (Epstein, 2008), and is sensitive to heading direction (Baumann and Mattingley, 2010; Marchette et al., 2014). Functional connections found here between optic flow sensitive regions and the RSC further establish a role for the RSC in updating position and orientation based on visual cues from optic flow.

In previous work, Sherrill et al. (2013) demonstrated that the posterior parietal cortex (PPC) was recruited during successful FPP navigation relying on self-motion processing. The current study demonstrates that the PPC has functional connections with left V3A, left V6 and right hMT+ during FPP navigation. Studies measuring single unit activity in primates (Sato et al., 2006) and hemodynamic responses in humans (Maguire et al., 1998; Rosenbaum et al., 2004; Spiers and Maguire, 2006) have suggested that the PPC plays a critical role in navigation by integrating position and self-movement information. Cells in the rodent PPC encode precise self-motion and acceleration states during free roaming in an open arena (Whitlock et al., 2012). Human neuroimaging data demonstrates that PPC was recruited during navigation to a goal suggesting a role in the coding and monitoring of response-based spatial information concerning distant locations (Spiers and Maguire, 2006; Spiers and Barry, 2015). The functional connections identified here between optic flow sensitive regions and the PPC may support integration of self-motion cues and planned route actions.

Another key finding in the present study was that left V3A, left and right V6, and right hMT+ seed regions had functional connections with the head and body of the right hippocampus during FPP navigation compared to the ITI. Functional connections between the hippocampus and optic flow regions during FPP navigation is consistent with computational models indicating that self-motion cues from optic flow might underlie coding of spatial position by grid cells and border cells in structures providing input to the hippocampus (Raudies et al., 2012; Raudies and Hasselmo, 2012). Some human lesion studies have not supported the idea that the hippocampus is necessary for path integration (Shrager et al., 2008; Kim et al., 2013), yet other neuropsychological studies found that patients with right hippocampal lesions had impairments in path integration without visual cues (Worsley et al., 2001; Philbeck et al., 2004). Additional patient studies have indicated that navigators with hippocampal lesions rely on extrahippocampal processes (context cues, object recognition) to support performance of landmark-based navigation (Kessels et al., 2011). The current study's results indicate that the hippocampus in conjunction with functional connections to optic flow sensitive regions plays a crucial role in using self-motion for FPP navigation.

Functional connections between bilateral V3A and V6 and right hMT+ seed regions and the medial prefrontal cortex were also found during successful FPP navigation compared to the ITI. Medial prefrontal involvement in the current task is consistent with its role in spatial

working memory (Wolbers et al., 2007; Arnold et al., 2014) and route navigation tasks (Spiers and Maguire, 2007). Wolbers et al. (2007) suggested that visual path integration is linked through interplay of self-motion processing in hMT+, higher-level spatial processes in the hippocampus, and spatial working memory in the medial prefrontal cortex. In support of that claim, our results establish a functional connection between right hMT+, the right hippocampus, and the bilateral medial prefrontal cortex during FPP navigation requiring path integration mechanisms.

Functional connections with optic flow sensitive regions during survey perspective navigation

When navigating in the Survey perspective, participants simply navigated the vehicle via the button box to the goal location maintained in short-term memory. During Survey perspective navigation, visual flow was minimal since the vehicle driven by our participants was the only movement on the screen. Tracking position in the environment via self-motion cues was not required as it was in FPP navigation. We found increased functional connectivity between visual cortical areas V3A, V6, and hMT+ and the primary motor cortex during Survey perspective navigation compared to the ITI. The contrast between the Survey perspective results and FPP results further strengthens our conclusion of functional interplay during FPP navigation between optic flow sensitive regions and brain regions required for navigation. Interestingly, our results demonstrated that the right V3A seed region demonstrated increased functional connectivity with the body of the right hippocampus and the right medial prefrontal cortex during Survey perspective navigation compared to the ITI. The functional connection between right V3A, hippocampus and medial prefrontal cortex may represent a functional integration of encoded spatial information required to implement a successful route towards a goal location, even when not tied to self-motion.

Conclusions

A functional link between optic flow sensitive regions and navigationally responsive regions has not yet been established in animals or humans. The current study provides this functional link. Previous neuroimaging research has established that cortical areas V3A, V6, and hMT+ process optic flow. Here, we examined functional connections between these optic flow sensitive regions and brain regions known to be important for navigation. The results demonstrate that goal-directed navigation requiring path integration mechanisms involves a cooperative interaction between optic flow sensitive regions V3A, V6, and hMT+ and the hippocampus, retrosplenial, posterior parietal and medial prefrontal cortices. These functional connections suggest a dynamic interaction between self-motion processing and navigationally responsive systems to support goal-directed navigation.

References

Andersson, J.L., Hutton, C., Ashburner, J., Turner, R., Friston, K., 2001. Modeling geometric deformations in EPI time series. NeuroImage 13, 903–919.

Arnold, A.E., Burles, F., Bray, S., Levy, R.M., Iaria, G., 2014. Differential neural network configuration during human path integration. Front. Hum. Neurosci. 8, 263.

Ashburner, J., 2007. A fast diffeomorphic image registration algorithm. NeuroImage 38, 95–113.

Baumann, O., Mattingley, J.B., 2010. Medial parietal cortex encodes perceived heading direction in humans. J. Neurosci. 30, 12897–12901.

Bremmer, F., Kubischik, M., Pekel, M., Hoffmann, K.P., Lappe, M., 2010. Visual selectivity for heading in monkey area MST. Exp. Brain Res. 200, 51–60.

Brown, T.I., Ross, R.S., Keller, J.B., Hasslemo, M.E., Stern, C.E., 2010. Which way was I going? Contextual retrieval supports the disambiguation of well learned overlapping navigational routes. Journal of Neuroscience 30, 7414–7422.

Brown, T.I., Stern, C.E., 2014. Contributions of medial temporal lobe and striatal memory systems to learning and retrieving overlapping spatial memories. Cereb. Cortex 24, 1906–1922.

Brown, T.I., Ross, R.S., Tobyne, S.M., Stern, C.E., 2012. Cooperative interactions between hippoampal and striatal systems support flexible navigation. NeuroImage 60, 1316–1330.

Cardin, V., Smith, A.T., 2010. Sensitivity of human visual and vestibular cortical regions to egomotion-compatible visual stimulation. Cereb. Cortex 20, 1964–1973.

Cardin, V., Smith, A.T., 2011. Sensitivity of human visual cortical area V6 to stereoscopic depth gradients associated with self-motion. J. Neurophysiol. 106, 1240–1249.

Chen, L.L., Lin, L.H., Green, E.J., Barnes, C.A., McNaughton, B.L., 1994. Head-direction cells in the rat posterior cortex. I. Anatomical distribution and behavioral modulation. Exp. Brain Res. 101, 8–23.

Cho, J., Sharp, P.E., 2001. Head direction, place, and movement correlates for cells in the rat retrosplenial cortex. Behav. Neurosci. 115, 3–25.

Chrastil, E.R., 2013. Neural evidence supports a novel framework for spatial navigation. Psychon. Bull. Rev. 20, 208–227.

Cooper, B.G., Mizumori, S.J., 2001. Temporary inactivation of the retrosplenial cortex causes a transient reorganization of spatial coding in the hippocampus. J. Neurosci. 21, 3986–4001.

Cooper, B.G., Manka, T.F., Mizumori, S.J., 2001. Finding your way in the dark: the retrosplenial cortex contributes to spatial memory and navigation without visual cues. Behav. Neurosci. 115, 1012–1028.

Doeller, C.F., Barry, C., Burgess, N., 2010. Evidence for grid cells in a human memory network. Nature 463, 657–661.

Dukelow, S.P., DeSouza, J.F., Culham, J.C., van den Berg, A.V., Menon, R.S., Vilis, T., 2001. Distinguishing subregions of the human MT+ complex using visual fields and pursuit eye movements. J Neurophysiol. 86, 1991–2000.

Duffy, C.J., 2009. Visual motion processing in aging and Alzheimer's disease: neuronal mechanisms and behavior from monkey to man. Ann. N. Y. Acad. Sci. 1170, 736–744.

Elduayen, C., Save, E., 2014. The retrosplenial cortex is necessary for path integration in the dark. Behav. Brain Res. 272, 303–307.

Epstein, R.A., 2008. Parahippocampal and retrosplenial contributions to human spatial navigation. Trends Cogn. Sci. 12, 388–396.

Fischer, E., Bulthoff, H.H., Logothetis, N.K., Bartels, A., 2012. Human areas V3A and V6 compensate for self-induced planar visual motion. Neuron 73, 1228–1240.

Foo, P., Warren, W.H., Duchon, A., Tarr, M.J., 2005. Do humans integrate routes into a cognitive map? Map- versus landmark-based navigation of novel shortcuts. J. Exp. Psychol. Learn. Mem. Cogn. 31, 195–215.

Fornito, A., Zalesky, A., Pantelis, C., Bullmore, E.T., 2012. Schizophrenia, neuroimaging, and connectiomics. NeuroImage 62, 2296–2314.

Gazzaley, A., Rissman, J., Cooney, J., Rutman, A., Seibert, T., Clapp, W., D'Esposito, M., 2007. Functional interactions between prefrontal and visual association cortex contribute to top-down modulation of visual processing. Cereb. Cortex 17, i125–i135.

Greicius, M.D., Supekar, K., Menon, V., Dougherty, R.F., 2009. Resting-state functional connectivity reflects structural connectivity in the default mode network. Cereb. Cortex 19, 72–78.

Hafting, T., Fyhn, M., Molden, S., Moser, M.B., Moser, E.I., 2005. Microstructure of a spatial map in the enthorhinal cortex. Nature 436, 801–806.

Hartley, T., Burgess, N., Lever, C., Cacucci, F., O'Keefe, J., 2000. Modeling place fields in terms of the cortical inputs to the hippocampus. Hippocampus 10, 369–379.

Hasselmo, M.E., 2009. A model of episodic memory: mental time travel along encoded trajectories using grid cells. Neurobiol. Learn. Mem. 92, 559–573.

Huk, A.C., Dougherty, R.F., Heeger, D.J., 2002. Retinotopy and functional subdivision of human areas MT and MST. J. Neurosci. 22, 7195–7205.

Kalia, A.A., Schrater, P.R., Legge, G.E., 2013. Combining path integration and remembered landmarks when navigating without vision. PLoS One 8, e72170.

Kearns, M.J., Warren, W.H., Duchon, A.P., Tarr, M.J., 2002. Path integration from optic flow and body senses in a homing task. Perception 31, 349–374.

Kessels, R.P., van Doormaal, A., Janzen, G., 2011. Landmark recognition in Alzheimer's dementia: spared implicit memory for objects relevant for navigation. PLoS One 6, e18611.

Kim, S., Sapiurka, M., Clark, R.E., Squire, L.R., 2013. Contrasting effects of path integration after hippocampal damage in humans and rats. Proc. Natl. Acad. Sci. U. S. A. 110, 4732–4737.

Lesh, T.A., Niendam, T.A., Minzenberg, M.J., Carter, C.S., 2011. Cognitive control deficits in schizophrenia: Mechanisms and meaning. Neuropsychopharmacology 36, 316–338.

Logan, D.J., Duffy, C.J., 2006. Cortical area MSTd combines visual cues to represent 3-D self-movement. Cereb. Cortex 16, 1494–1507.

Maguire, E.A., Burgess, N., Donnett, J.G., Frackowiak, R.S., Frith, C.D., O'Keefe, J., 1998. Knowing where and getting there: a human navigation network. Science 280, 921–924.

Marchette, S.A., Vass, L.K., Ryan, J., Epstein, R.A., 2014. Anchoring the neural compass: coding of local spatial reference frames in human medial parietal lobe. Nat. Neurosci. 17, 1598–1606.

May, M., Klatzky, R.L., 2000. Path integration while ignoring irrelevant movement. J. Exp. Psychol. Learn. Mem. Cogn. 26, 169–186.

McNaughton, B.L., Battaglia, F.P., Jensen, O., Moser, E.I., Moser, M.B., 2006. Path integration and the neural basis of the 'cognitive map'. Nat. Rev. Neurosci. 7, 663–678.

O'Keefe, J., Dostrovsky, J., 1971. The hippocampus as a spatial map: preliminary evidence from unit activity in the freely-moving rat. Brain Res. 34, 171–175.

Peuskens, H., Sunaert, S., Dupont, P., Van Hecke, P., Orban, G.A., 2001. Human brain regions involved in heading estimation. J. Neurosci. 21, 2451–2461.

Philbeck, J.W., Behrmann, M., Levy, L., Potolicchio, S.J., Caputy, A.J., 2004. Path integration deficits during linear locomotion after human medial temporal lobectomy. J. Cogn. Neurosci. 16, 510–520.

Pitzalis, S., Galletti, C., Huang, R.S., Patria, F., Committeri, G., Galati, G., Fattori, P., Sereno, M.I., 2006. Wide-field retinotopy defines human cortical visual area v6. J. Neurosci. 26, 7962–7973.

Pitzalis, S., Sereno, M.I., Committeri, G., Fattori, P., Galati, G., Patria, F., Galletti, C., 2010. Human v6: the medial motion area. Cereb. Cortex 20, 411–424.

Pothuizen, H.H., Aggleton, J.P., Vann, S.D., 2008. Do rats with retrosplenial cortex lesions lack direction? Eur. J. Neurosci. 28, 2486–2498.

Putcha, D., Ross, R., Rosen, M., Norton, D., Cronin-Golomb, A., Somers, D., Stern, C., 2014. Functional correlates of optic flow motion processing in Parkinson's disease. Front. Integr. Neurosci. 8, 57–72.

Raudies, F., Hasselmo, M.E., 2012. Modeling boundary vector cell firing given optic flow as a cue. PLoS Comput. Biol. 8, e1002553.

Raudies, F., Mingolla, E., Hasselmo, M.E., 2012. Modeling the influence of optic flow on grid cell firing in the absence of other cues. J. Comput. Neurosci. 33, 475–493.

Rissman, J., Gazzaley, A., D'Esposito, M., 2004. Measuring functional connectivity during distinct stages of a cognitive task. NeuroImage 23, 752–763.

Rosenbaum, R.S., Ziegler, M., Winocur, G., Grady, C.L., Moscovitch, M., 2004. "I have often walked down this street before": fMRI studies on the hippocampus and other structures during mental navigation of an old environment. Hippocampus 14, 826–835.

Ross, R.S., Brown, T.I., Stern, C.E., 2009. The retrieval of learned sequences engages the hippocampus: evidence from fMRI. Hippocampus 19, 790–799.

Rust, N.C., Mante, V., Simoncelli, E.P., Movshon, J.A., 2006. How MT cells analyze the motion of visual patterns. Nat. Neurosci. 9, 1421–1431.

Sato, N., Sakata, H., Tanaka, Y., Taira, M., 2006. Navigation-associated medial parietal neurons in monkeys. Proc. Natl. Acad. Sci. U. S. A. 103, 17001–17006.

Scholvinck, M.L., Maier, A., Ye, F.Q., Duyn, J.H., Leopold, D.A., 2010. Neural basis of global resting-state fMRI activity. Proc. Natl. Acad. Sci. U. S. A. 107, 10238–10243.

Seiffert, A.E., Somers, D.C., Dale, A.M., Tootell, R.B.H., 2003. Functional MRI studies of human visual motion perception: texture, luminance, attention and after-effects. Cereb. Cortex 13, 340–349.

Sherrill, K.R., Erdem, U.M., Ross, R.S., Brown, T.I., Hasselmo, M.E., Stern, C.E., 2013. Hippocampus and retrosplenial cortex combine path integration signals for successful navigation. J. Neurosci. 33, 19304–19313.

Shrager, Y., Kirwan, C.B., Squire, L.R., 2008. Neural basis of the cognitive map: path integration does not require the hippocampus or medial entorhinal cortex. Proc. Natl. Acad. Sci. U. S. A. 105, 12034–12038.

Spiers, H.J., Barry, C., 2015. Neural systems supporting navigation. Current Opinion in Behavioral Sciences 1, 47–55.

Spiers, H.J., Maguire, E.A., 2006. Thoughts, behavior, and brain dynamics during navigation in the real world. NeuroImage 31, 1826–1840.

Spiers, H.J., Maguire, E.A., 2007. A Navigational Guidance System in the Human Brain. Hippocampus 17, 618–626.

Straw, A.D., 2008. Vision egg: an open-source library for reltime visual stimulus generation. Front Neuroinform 2, 4.

Swisher, J.D., Halko, M.A., Merabet, L.B., McMains, S.A., Somers, D.C., 2007. Visual topography of human intraparietal sulcus. J. Neurosci. 27, 5326–5337.

Taube, J.S., Muller, R.U., Ranch Jr., J.B., 1990. Head-direction cells recorded from the postsubiculum in freely moving rats. J. Neurosci. 10, 420–435.

Tcheang, L., Bulthoff, H.H., Burgess, N., 2011. Visual influence on path integration in darkness indicates a multimodal representation of large-scale space. Proc. Natl. Acad. Sci. U. S. A. 108, 1152–1157.

Tootell, R.B., Mendola, J.D., Hadjikhani, N.K., Ledden, P.J., Liu, A.K., Reppas, J.B., Sereno, M.I., Dale, A.M., 1997. Functional analysis of V3A and related areas in human visual cortex. J. Neurosci. 17, 7060–7078.

Wandell, B.A., Dumoulin, S.O., Brewer, A.A., 2007. Visual field maps in human cortex. Neuron 56, 366–383.

Weiner, J., Berthoz, A., Wolbers, T., 2011. Dissociable cognitive mechanisms underlying path integration. Exp. Brain Res. 208, 61–71.

Whitlock, J., Pfuhl, G., Dagslott, N., Moser, M.B., Moser, E.I., 2012. Functional split between parietal and entorhinal cortices in the rat. Neuron 73, 789–802.

Wolbers, T., Buchel, C., 2005. Dissociable retrosplenial and hippocampal contributions to successful formation of survey representations. J. Neurosci. 25, 3333–3340.

Wolbers, T., Wiener, J.M., Mallot, H.A., Buchel, C., 2007. Differential recruitment of the hippocampus, medial prefrontal cortex, and the human motion complex during path integration in humans. J. Neurosci. 27, 9408–9416.

Worsley, C.L., Recce, M., Spiers, H.J., Marley, J., Polkey, C.E., Morris, R.G., 2001. Path integration following temporal lobectomy in humans. Neuropsychologia 39, 452–464.